ACS APPLIED MATERIALS & INTERFACES

www.acsami.org

Research Article

Interfacial Distribution of Nafion Ionomer Thin Films on Nitrogen-Modified Carbon Surfaces

Wataru Yoshimune,* Nobuaki Kikkawa,* Hiroaki Yoneyama, Naoko Takahashi, Saori Minami, Yusuke Akimoto, Takuya Mitsuoka, Hiroyuki Kawaura, Masashi Harada, Norifumi L. Yamada, and Hiroyuki Aoki

Cite This: *ACS Appl. Mater. Interfaces* 2022, 14, 53744−53754

Read Online

ACCESS | Metrics & More | Article Recommendations | Supporting Information

ABSTRACT: Chemically modified carbon supports for the cathode catalyst layers of polymer electrolyte fuel cells (PEFCs) show considerable promise for boosting the oxygen reduction reaction. This study evaluated the ionomer distribution of Nafion ionomer thin films on nitrogen (N)-modified carbon surfaces along their depth direction. Neutron reflectivity (NR) measurements performed using the double-contrast technique with H_2O and D_2O revealed that the introduction of N functional groups to carbon thin films promoted ionomer adsorption onto the surface under wet conditions (22 °C, 85% relative humidity). Molecular dynamics (MD) simulations conducted to verify the origin of the robust contact between the ionomer and N-modified carbon surface revealed an ionomer adsorption mechanism on the N-modified carbon surfaces, which involved Coulomb interactions between the positively charged carbon surface and the ionomer side chains with negatively charged sulfonic acid groups. The positive surface charge, which was determined using the contents of the N functional groups estimated by X-ray photoelectron spectroscopy, was found to be sufficient as an impetus for ionomer adsorption. This strategy involving NR measurements and MD simulations can provide insights into the solid−ionomer interfacial structures in a cathode catalyst layer and can therefore be extensively employed in studies on PEFCs.

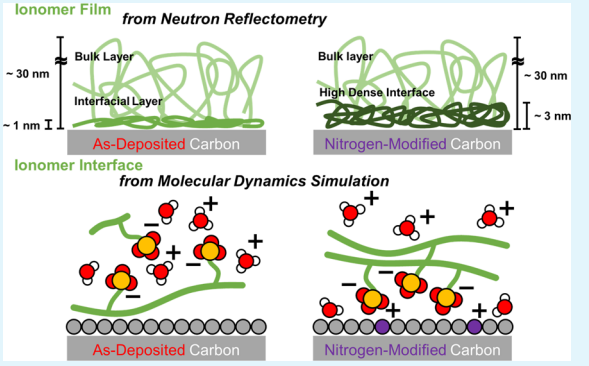

KEYWORDS: *polymer electrolyte fuel cell, nitrogen-modified carbon surface, ionomer distribution, neutron reflectometry, molecular dynamics simulation*

INTRODUCTION

Polymer electrolyte fuel cells (PEFCs) have been studied over the last three decades for automobile applications,[1] in particular, fuel-cell electric vehicles (FCEVs), which have been commercially available since 2014.[2] To satisfy the demand for lower prices, the Pt loading in the cathode catalyst layer of FCEVs must be preferentially reduced by enhancing the Pt mass activity for the oxygen reduction reaction (ORR). Remarkable advances have recently been made in the development of ORR-active nanostructured cathode catalysts with controlled size, composition, morphology, or shape.[3−5] Furthermore, heteroatoms introduced into the carbon support enhance ORR activity and durability[6,7] via interfacial geometric interactions at Pt−C interfaces,[8,9] thereby potentially contributing to the reduction of Pt loading in FCEVs.

A perfluorinated sulfonic acid polymer—called an ionomer—is typically included in the catalyst layers of PEFCs to improve proton conductivity.[1] However, the ionomer addition is known to induce detrimental effects. For instance, the sulfonate anions of the side chains in the ionomer adsorb onto the Pt surface, leading to a reduction in ORR activity;[10−13] this is referred to as ionomer poisoning. It should be mentioned here that some reports showed that the sulfonate anions positively affect ORR activity and durability.[14−17] Additionally, the presence of a dense ionomer layer near the Pt surface deteriorates the local O_2-transport properties.[18−21] Therefore, ionomer-free nanostructured thin-film catalyst layers have been developed by the 3M Company to prevent these detrimental effects.[22] However, their performance is insufficient from the viewpoint of FCEV commercialization because of their low proton conductivity, especially under low-humidity conditions.[23] Therefore, the coexistence of Pt and ionomers in the catalyst layers of FCEVs is unavoidable.

Yarlagadda et al. used accessible porous carbon to mitigate the trade-off-related issues due to the ionomer addition.[24] Accessible porous carbon can be effective in this regard

Received: August 16, 2022
Accepted: November 11, 2022
Published: November 23, 2022

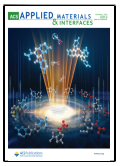

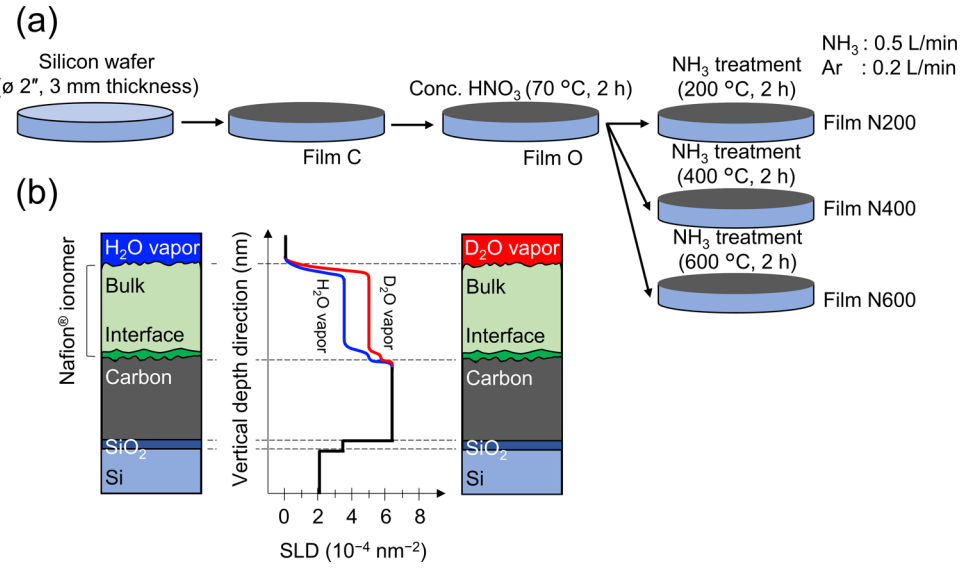

Figure 1. (a) Fabrication of surface-modified carbon thin films. (b) Schematic illustration of the overall system and the vertical scattering length density (SLD) profiles.

because the diameter of Pt-nanoparticle-embedded carbon pores is sufficiently small to suppress ionomer penetration, but not so small as to inhibit O_2 transport through the pores. Alternatively, ionomers with high O_2 permeability can be employed to reduce the O_2-transport resistance.[25−28] The framework of ionomers, which includes a ring-structured backbone with an O_2-permeable glassy amorphous matrix, improves the fuel cell performance without any noteworthy concerns.

The introduction of nitrogen to the surface of carbon supports has been proposed as an approach to distribute ionomers throughout the catalyst uniformly and thereby prevent ionomer poisoning and the formation of a dense ionomer layer at the Pt−ionomer interface.[29−36] This approach is fascinating because it involves the use of low-cost conventional materials. Orfanidi et al.[29] claimed that carbon supports modified by NH_3 treatment to have $-NH_x$ groups on their surface achieved a uniform ionomer distribution via Coulombic interactions with the negatively charged ionomer side chains (SO_3^-). Ott et al.[31] introduced balanced quantities of pyridinic/pyrrolic/graphitic nitrogen (N) functional groups that interacted with ionomer chains, which promoted their homogeneous spatial distribution. Matsutori et al.[33] demonstrated that pyrrolic N functional groups could be selectively and directly introduced to carbon supports using a grafting method that is initiated by the thermal decomposition of azo compounds in water. Electrochemical evaluations of N-modified carbon supports obtained via different synthetic routes have corroborated the strategy of using chemically modified carbon supports.

However, the interfacial structure between the N-modified carbon and ionomers has not been experimentally investigated to date; thus, the effects of this interface remain unclear. Therefore, the present study was aimed at unveiling the characteristics of the interfacial ionomer structure on a N-modified carbon surface and discussing the impact of the surface properties. The surfaces of ∼50-nm-thick carbon thin films deposited on Si wafers were chemically modified. Figure 1a shows the fabrication procedure (details provided in the Experimental Section) and sample notations. Heating temperatures of 200, 400, and 600 °C for NH_3 treatment, following parameters conducted by Ott et al.,[31] were used to control the amount of N species. The hydrophobic carbon surface (Film C) became a hydrophilic surface through chemical modifications (Films O, N200−N600). Approximately 30-nm-thick ionomer thin films were deposited onto the carbon films by spin-coating a Nafion ionomer dispersion, followed by annealing at 120 °C. We selected the annealing temperature assuming a hot-pressing temperature applied during the fabrication process of catalyst-coated membranes. In this work, Films C and N600 have been used for comparison in many of the analyses because Ott et al. reported that the use of N-modified carbon supports treated at 600 °C showed the best electrochemical performance.[31]

Neutron reflectivity (NR) measurements were performed to elucidate the interfacial ionomer structure on the N-modified carbon surfaces, as they can yield a vertical scattering length density (SLD) profile of the ionomer on carbon surfaces (Figure 1b). NR data were taken with two scattering contrasts on the same film using H_2O and D_2O vapor (double-contrast method). The relative humidity (RH) was set at ∼80%, a typical operating condition for PEFCs. The double-contrast method allows quantitative evaluation of the volume fraction of water penetrating the Nafion ionomer thin films from the difference in the SLD profiles (red and light blue lines in Figure 1b). Moreover, from the volume conservation, the volume fraction of the ionomer was evaluated in the thin films. The details of the evaluation method are provided in the Results and Discussion section. Additionally, molecular dynamics (MD) simulations were carried out to discuss the origin of driving forces for the ionomer structure at the carbon−ionomer interface.

RESULTS AND DISCUSSION

Surface Morphologies of Carbon Thin Films. Figure 2a,b shows scanning electron microscopy (SEM) images of the carbon surface on Films C and N600, respectively. These surfaces were observed to be crack-free. Carbon particles with diameters of several nanometers were observed, and their scale corresponded to the primary particle size of typical carbon

https://doi.org/10.1021/acsami.2c14574
ACS Appl. Mater. Interfaces 2022, 14, 53744−53754

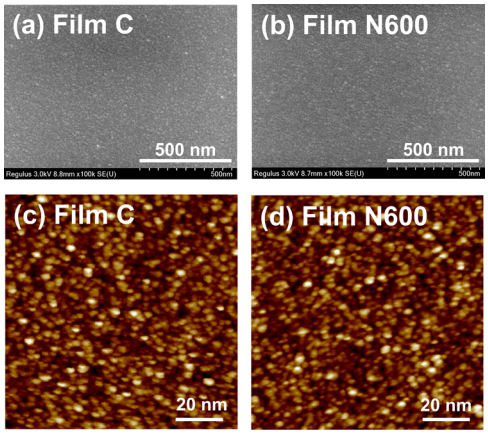

Figure 2. (a, b) Surface SEM images captured by the secondary electron mode and (c, d) tapping-mode AFM images of carbon thin films.

black employed as the carbon support in catalyst layers.[29−36] Surface AFM images (Figure 2c,d) show that the slight increase in surface roughness from Film C to Film N600 indicates that the NH_3 treatment damaged the carbon surface (see Table S1 for roughness parameters). Additionally, water contact angle measurements showed that Film C had a hydrophobic nature, but it became hydrophilic nature by HNO_3 and NH_3 treatments (Figure S1 and Table S2).

Compositional Analysis of Carbon Thin Films. X-ray photoelectron spectroscopy (XPS) was performed to elucidate the chemical compositions of the carbon thin films. The corresponding atomic compositions (Table 1) indicated that

Table 1. XPS-Based Compositional Analysis of Surface-Modified Carbon Thin Films

	composition (atomic %)[a]		
sample film	C 1s	O 1s	N 1s
C	87.8	10.7	1.4
O	86.2	11.9	1.3
N200	88.5	7.6	3.8
N400	88.0	5.1	6.8
N600	86.7	3.3	9.8

[a]The quantitative accuracy is two to three significant digits.

the carbon thin films consisted mainly of carbon, oxygen, and nitrogen. The carbon concentration of the thin films was in the 86−89 atomic% range. The oxygen concentration in Film O was greater than that in Film C because the HNO_3 treatment promoted surface functionalization with carboxylic, hydroxyl, and NO_x groups.[37] Moreover, the values corresponding to Films N200−N600 indicated that the oxygen concentration decreased and the nitrogen concentration increased with increasing NH_3 treatment temperature. These findings suggest that the NH_3 treatment replaced the O functional groups with N functional groups.[29−36]

Increasing peak intensities were observed in the N 1s XPS profiles (Figure 3), which indicated an increase in nitrogen concentration, as shown in Table 1; the C 1s and O 1s spectra are shown in Figure S2. Moreover, as the treatment temperature increased, the peak position shifted toward lower binding energies, indicating that the composition of the N functional groups changed. The N 1s XPS profiles were

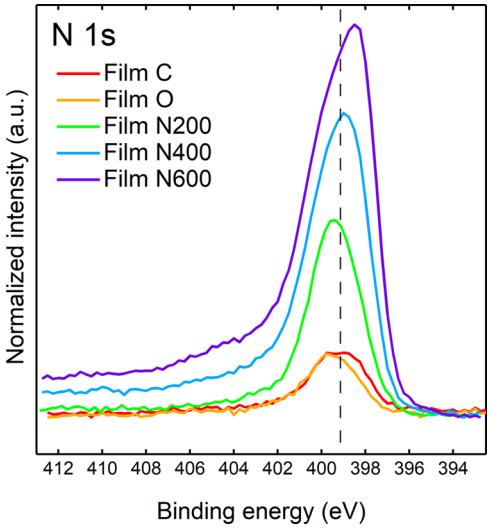

Figure 3. N 1s XPS profiles of carbon thin films. The dotted line indicates the peak corresponding to Film C and highlights the peak shifts with increasing NH_3-treatment temperature.

decomposed (Figure S3) to categorize the nitrogen concentration between six N functional groups: graphitic, quaternary, pyrrolic, pyridinic, NO_2, and NO_3 (Figure S4a and Table S3), in accordance with a study conducted by Ott et al.[31] Analysis of the proportion of each N functional group (Figure S4b) suggested that at lower NH_3 treatment temperatures, the majority of the N functional groups were pyrrolic, whereas at higher treatment temperatures, the proportions of pyridinic and quaternary groups increased. These changes in functionality are consistent with the results reported by Otto et al.[31]

In terms of Raman analysis (Figure 4), sharp peaks originating from the Si wafer were observed at 520 and 960 cm^{-1} in all of the sample spectra, in addition to a broad peak in the range of 1100−1800 cm^{-1}, which was ascribed to the carbon structure. The G band (~1500 cm^{-1}) in graphene

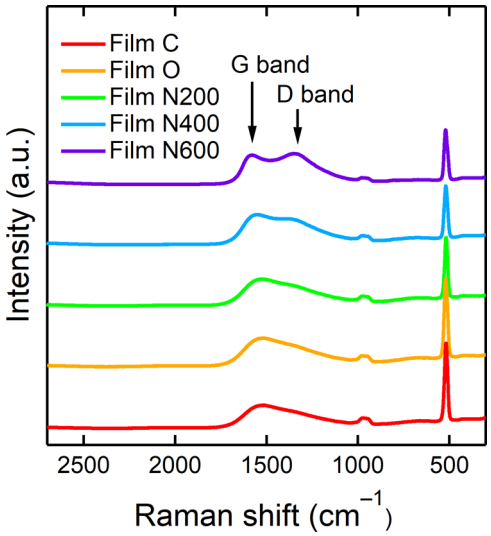

Figure 4. Raman spectra of the carbon thin films. The low-wavelength sharp peaks at 520 and 960 cm^{-1} and the high-wavelength broad peak originate from the Si wafer and carbon thin film, respectively. The G and D bands are induced by the carbon structure (~1500 and 1300 cm^{-1}, respectively; depicted by arrows).

https://doi.org/10.1021/acsami.2c14574
ACS Appl. Mater. Interfaces 2022, 14, 53744−53754

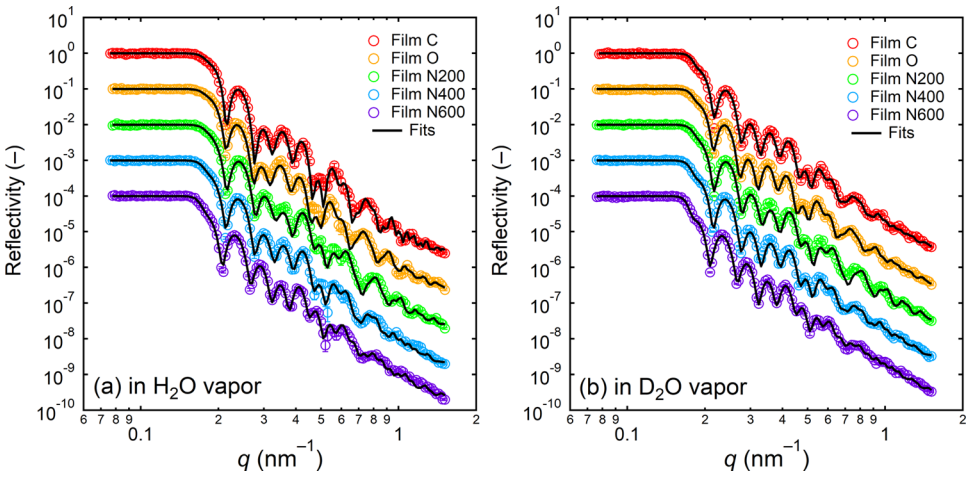

Figure 5. Experimental NR data and the corresponding fits (solid lines) of Nafion ionomer thin films obtained under (a) H_2O and (b) D_2O vapors. The NR curves have been vertically offset ($\times10^{-1}$, $\times10^{-2}$, $\times10^{-3}$, and $\times10^{-4}$ for Films O, N200, N400, and N600, respectively) to aid visualization.

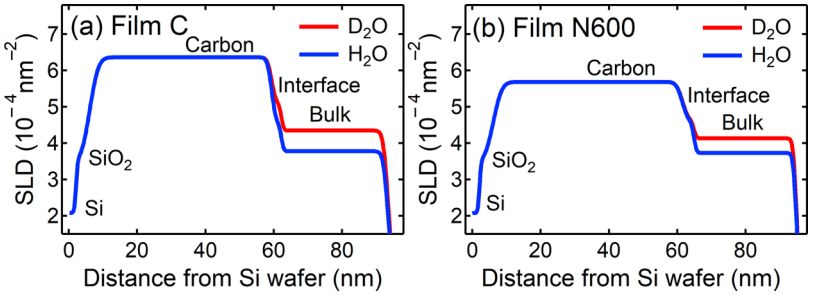

Figure 6. SLD profiles of the Nafion ionomer thin films on (a) Film C and (b) Film N600 acquired under H_2O (blue) and D_2O vapors (red).

represents in-plane vibrations, whereas disorders activate the D band (~1300 cm^{-1}) in sp^2 carbon clusters by the NH_3 treatment above 400 °C. Carbon thin films are graphitic and do not have the same physicochemical properties as amorphous carbon black used in fuel cells. The D/G ratio, which compares the relative areas of the D and G bands, is a well-established parameter for estimating the degree of lattice defects in graphene-like planes. The D/G ratios of Films C, O, N200, N400, and N600 were 0.42 ± 0.01, 0.41 ± 0.01, 0.37 ± 0.01, 0.28 ± 0.01, and 0.28 ± 0.01, respectively. The sudden decrease in the D/G ratio indicated that the NH_3 treatment at elevated temperatures (>400 °C) induced several tens of percent of defects in the framework of a graphene-like plane.

NR Measurements. Figure 5 shows the NR curves of the Nafion ionomer thin films obtained at 85% relative humidity (RH). The fringes observed in the NR curves originate from the interference of reflections at the interfaces in thin films. The shape of the fringes at q = ~0.55 nm^{-1} differed between Films C, O, and N200–N600, indicating changes in the ionomer-related interfacial structures on the N-modified carbon surfaces. The difference is discussed quantitatively in the next section. Figure S5 shows the NR curves of thin films that were subjected to one and two drying cycles. The NR curves of all of the samples obtained after the repeated drying overlapped, indicating that the ionomer migration routinely observed in fuel cells operating under wet/dry cycles[38] was negligible in our system. The annealing history of ionomer thin films can significantly alter the structure of ionomers. A repeated wet/dry cycle may not relax the structure unless the film is treated with liquid water, as discussed by Paul and Karan.[39] In a fuel cell, liquid water will be produced, which can relax and plasticize the ionomer and alter the interfacial characteristics.

For quantitative assessment, the experimental NR curves were fitted to a structural model described in Figure 1b using the least-squares method. The NR curves of the thin films acquired under H_2O vapor were first analyzed to determine the structural parameters of the carbon and Nafion ionomer layers, such as the thickness, SLD, and interfacial roughness. In the fits to the NR data obtained under D_2O vapor, only the SLDs of the ionomer thin films were fitted using the parameters determined by fitting the NR curves collected under H_2O vapor. An "interfacial layer" (Figure 1b) was added on the side of the carbon in the bulk Nafion ionomer layer, in accordance with the literature.[20,40–48] Initially, a water-rich layer on the carbon surface was considered, as has been extensively reported for SiO_2–Nafion and Pt–Nafion interfaces.[41,42,44–46] However, this assumption could not reproduce the NR curves. Therefore, a high dense Nafion ionomer layer[20,40] was considered, which improved the goodness of fit (see the Supporting Information for details).

The SLD profiles of Films C and N600 corresponding to the optimal fitting results (Figure 6) showed a dependence on the vertical distance from the Si surface, indicating fluctuations in the density and/or composition of the thin films. The SLD value at the origin of the vertical axis (2.07×10^{-4} nm^{-2}) corresponded to Si. Moreover, several nanometers of native SiO_2 layer were present on the surface of the Si layer (SLD = 3.47×10^{-4} nm^{-2}). In this study, the structural parameters of Si and its native oxide layer (SiO_2) were assumed to be identical for all samples. As mentioned earlier, an ~50-nm-thick carbon film was present on the SiO_2 layer. The SLD of

https://doi.org/10.1021/acsami.2c14574
ACS Appl. Mater. Interfaces 2022, 14, 53744–53754

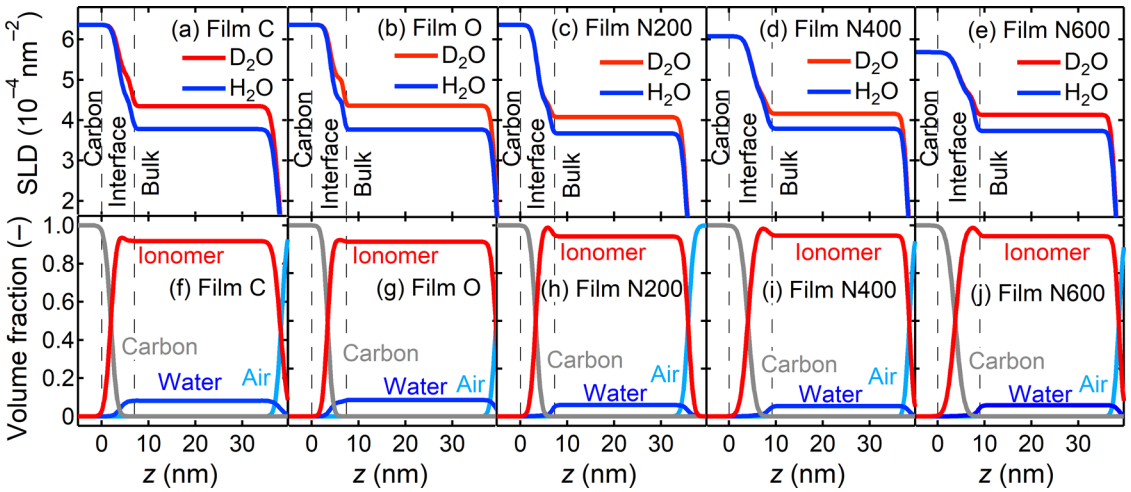

Figure 7. (a–e) SLD profiles of Nafion ionomer thin films as a function of vertical distance from the carbon surface z obtained under H_2O (blue) and D_2O vapors (red). (f–j) Volume fractions of the components of the Nafion ionomer thin films. Gray, red, blue, and light blue lines represent carbon, the Nafion ionomer, water, and air, respectively.

the carbon film in Film C, which was utilized as a fitting parameter, matched that of bulk carbon ($SLD_C = 6.36 \times 10^{-4}$ nm^{-2}). However, the SLD of the carbon layer in Film N600 decreased to 5.68×10^{-4} nm^{-2} upon the NH_3 treatment. The critical angle of total reflection in the NR data (Figure S6a) qualitatively indicates that the SLD of the N-modified carbon layer is lower than that of the as-deposited carbon layer. We double-checked the density and thickness of carbon thin films using laboratory X-ray reflectivity (XRR) measurements. As a result of XRR data analysis (see Table S4), we validated the reduction in SLD of the carbon layers after NH_3 treatment. When nitrogen atoms are incorporated into a carbon film, the SLD increases because the scattering length of nitrogen atoms is larger than that of carbon atoms. The decrease in the SLD of Film N600 can be explained by the introduction of voids ($SLD_V = 0$ nm^{-2}) to the carbon thin films, which corresponds to the formation of ~10% voids by volume fraction. The water contact angle measurements (Figure S1 and Table S2) show that the hydrophobic nature changed to hydrophilic after the treatment. Open hydrophilic pores on the carbon surface will be filled with water driven by the capillary force. Figure S6b,c shows the critical angles of total reflection in the NR data for Film C and Film N600 under dry or water vapor exposure (H_2O and D_2O). There is no sign of changes in the critical angle under conditions, ignoring the possibility of SLD changes due to water filling into the hydrophilic voids of the carbon layers. The SEM and AFM observations (Figure 2) confirmed the absence of cracks on the carbon surface, indicating that the voids were not caused by cracks. The degree of lattice defects estimated using the Raman spectra was roughly consistent with the decrease in the density elucidated by XRR and NR analysis (Figure S7). Therefore, the decrease in the SLD of the carbon layer in Film N600 could be explained by the presence of lattice defects in the graphene-like plane of the carbon layer. Lattice defects (such as point defects, edge defects, and structural distortions) attributed by Raman spectroscopy[49] will be too small to be filled with water.

The SLD profiles (Figure 6) involve contributions from several components, as follows

$$SLD_{film}^{H_2O} = \varphi_W SLD_{H_2O} + \varphi_N SLD_N + \varphi_C SLD_C + \varphi_A SLD_A \quad (1)$$

$$\varphi_W + \varphi_N + \varphi_C + \varphi_A = 1 \quad (2)$$

where $SLD_{film}^{H_2O}$, SLD_{H_2O} ($= -0.56 \times 10^{-4}$ nm^{-2}), SLD_N, and SLD_A ($= 0$ nm^{-2}) are the SLDs of a film under H_2O vapor, H_2O, the Nafion ionomer, the carbon layer, and the air/voids in the film, respectively; and φ_W, φ_N, φ_C, and φ_A are the volume fractions of water, the Nafion ionomer, carbon, and air/voids, respectively. To quantitatively examine the water distribution in the thin films, φ_W was determined using the double-contrast method. Substituting D_2O for H_2O increased the SLDs of ionomer layers (Figure 6) because of the difference between the SLDs of the water incorporated by the layers. The following equation applies in the H_2O and D_2O double-contrast NR measurements

$$SLD_{film}^{H_2O} - SLD_{film}^{D_2O} = \varphi_W(SLD_{H_2O} - SLD_{D_2O}) \quad (3)$$

where $SLD_{film}^{D_2O}$ and SLD_{D_2O} ($= 6.37 \times 10^{-4}$ nm^{-2}) are the SLD of the films measured under D_2O vapor and D_2O, respectively. The φ_W values of the ionomer layers can be definitively determined using the double-contrast method from the SLD profiles without any assumptions because the two to four terms in eq 1 are eliminated by subtraction. However, certain assumptions are required to evaluate both SLD_N and φ_N. The volume fraction of the ionomer in the films was evaluated under the following assumptions: (i) the volume fraction of carbon in the carbon–ionomer interface that originated from the roughness was considered,[40] as discussed in the Supporting Information; (ii) the volume fractions of carbon and voids in the ionomer layers were assumed to be zero; (iii) SLD_N was fluctuated to accommodate the aforementioned assumptions and eq 2; and (iv) the volume fraction of air in the ionomer–air interface was determined for satisfying eqs 1 and 2. Assumption (iii) considers the variation in ionomer volume per molecule, v_0 (nm^3), due to the packing degree of the polytetrafluoroethylene backbone.[50]

The volume fraction of each component was evaluated based on the aforementioned assumptions. Figure 7 shows SLD profiles and volume fractions of the Nafion ionomer thin films as a function of the vertical distance from the carbon surface. All fitting parameters are summarized in Table S5. For all samples, the SLD_N value of the ionomer layers was varied

https://doi.org/10.1021/acsami.2c14574
ACS Appl. Mater. Interfaces 2022, 14, 53744–53754

from 3.95×10^{-4} to 4.17×10^{-4} nm^{-2} with different ν_0 based on assumption (iii), which was within ±5% of the ν_0 (0.79 nm^3) in Nafion ionomer.[40]

The φ_C in the carbon surface decayed over several nanometers of the vertical distance owing to the roughness, and the extent of this decay increased slightly from Films C to N600 because of the damage induced by the NH_3 treatment. This trend is consistent with the surface roughness as evaluated by topographic AFM images and XRR measurements (Tables S1 and S4). At the carbon−ionomer interface, the "ionomer adsorption layer" appeared as φ_N increased compared with that of the bulk layer (red profiles at the interface in Figure 7f−j). The hydrophobic carbon surface (Film C) had an ∼1-nm-thin ionomer adsorption layer, whereas the hydrophilic carbon surface (Film O) nearly disappeared from the adsorption layer. This discrepancy was presumably caused by the fact that the ionomer backbone, which was present as rod-shaped aggregates in the bulk, was adequately adsorbed onto the hydrophobic carbon surface after the hydrophobic interactions ruptured the aggregates.[51] Moreover, the thickness and volume fraction of the ionomer in the ionomer adsorption layer increased after the NH_3 treatment (Films N200−N600) compared with those of Films C and O. Instead of the appearance of the dense ∼3-nm-thick ionomer layer in Films N200−N600, a decrease in φ_W at the interface was observed compared to that of Films C and O (Table 2). As shown in Figure 7c−e, the overlap of the $SLD_{film}^{H_2O}$ (blue) and $SLD_{film}^{D_2O}$ (red) profiles at the carbon−ionomer interface visually confirmed the loss of water. Additionally, the water content decreased not only at the interface but also throughout the thin films (see Bulk Layer in Table 2). For comparison with the data summarized in certain review articles,[52,53] the φ_W values at the bulk and interfacial layers were converted to water uptake based on a commonly used parameter called λ_W, which is defined as the number of water molecules per sulfonic group of the ionomer. The swelling ratio ($\Delta L/L_0$) was calculated using the total thickness of the bulk and interfacial layers in the dry/wet ionomer films that were estimated from the fitted NR profiles. These physicochemical properties are summarized in Table 2. Compared to the λ_W of a bulk Nafion membrane[52] (10−15 at 22 °C), <100-nm-thick Nafion films have been shown to exhibit low λ_W values owing to a "thin-film effect." Ionomer thin films of 30 nm thickness have been reported to show λ_W values of 1.8−3.2 at 20−25 °C and 75% RH.[51] Moreover, a thin-film effect has also been observed in terms of swelling thickness, and the results reported herein are reasonably consistent with those of previous studies.[52] The NR measurements suggested that the water uptake properties deteriorated upon NH_3 treatment, particularly in the interfacial layer (Table 2). This feature implies that the fuel cell performance achieved using N-modified carbon in the cathode catalyst layers can be reduced owing to the reduction in water uptake when operated under low-humidity conditions.

Table 2. Physicochemical Properties of Nafion Ionomer Thin Films on Carbon Surfaces[b]

film	layer	φ_W (−)[a]	λ_W (−)[a]	$\Delta L/L_0$ (%)[a]
C	bulk	0.08 ± 0.02	2.3 ± 0.1	9.6 ± 0.1
	interface	0.08 ± 0.02	2.3 ± 0.1	
O	bulk	0.09 ± 0.02	2.5 ± 0.1	9.0 ± 0.1
	interface	0.08 ± 0.02	2.2 ± 0.1	
N200	bulk	0.06 ± 0.02	1.7 ± 0.1	6.6 ± 0.7
	interface	0.001 ± 0.001	0.04 ± 0.02	
N400	bulk	0.05 ± 0.02	1.5 ± 0.1	8.4 ± 0.2
	interface	0.009 ± 0.002	0.23 ± 0.01	
N600	bulk	0.06 ± 0.01	1.6 ± 0.1	7.1 ± 0.2
	interface	0.006 ± 0.002	0.17 ± 0.01	

[a]± is defined as the error propagation calculated to account for errors in the parameters determined by the fitting of NR profiles. [b]φ_W, λ_W, and $\Delta L/L_0$ represent the volume fraction of water, water uptake, and swelling ratio, respectively.

MD Simulation. N-modified carbon is a hydrophilic surface (Figure S1 and Table S2), and the morphology of the ionomer adsorption layer depends on the wettability of the carbon surface.[51,54] A water-rich layer exists near the hydrophilic carbon surface treated with ultraviolet irradiation in wet ionomer thin films.[40] However, the NR experiments reported herein suggest the presence of a thick and dense ionomer without a water-rich layer on the N-modified carbon surface. Therefore, we confirmed the validity of the interfacial structure using MD simulations. Figure 8 shows the distributions of the F atoms in the Nafion ionomer and the O atoms in water and hydronium ions (except in the Nafion ionomer) on the (a) hydrophobic as-deposited (corresponding to Film C) and (b) hydrophilic N-modified (corresponding to Film N200) carbon surfaces. In the as-deposited carbon surface, water was found to be uniformly distributed in the ionomer thin film with an ionomer-rich topmost layer (∼0.6 nm) near the carbon surface. For the N-modified carbon surface, the presence of a water-rich layer as water molecules rather than hydronium ions was confirmed at the topmost layer (∼5 Å) on the carbon surface (see Figures 8 and S11). A dense ∼2-nm-thick ionomer layer was formed on the water-rich layer, indicating that SO^{3-} groups in the ionomer were tightly

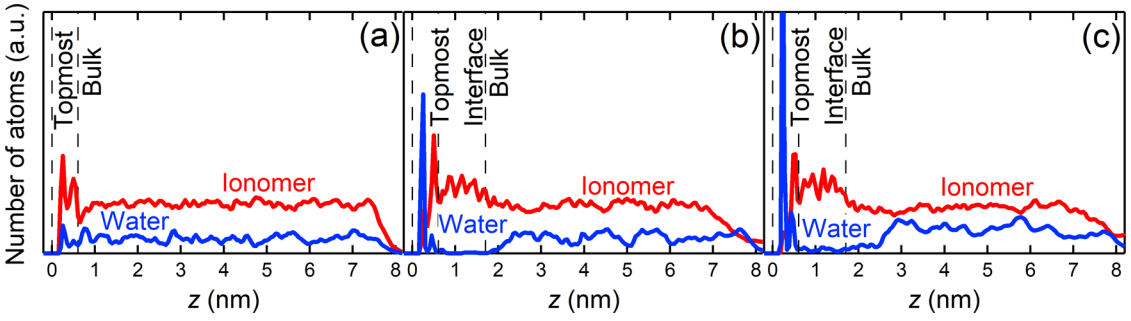

Figure 8. Number of F atoms (red) in the Nafion ionomer and O atoms (blue) in water and hydronium ions for the ionomer thin films on the (a) as-deposited, (b) N-modified, and (c) hydrophobic positively charged carbon surfaces.

https://doi.org/10.1021/acsami.2c14574
ACS Appl. Mater. Interfaces 2022, 14, 53744−53754

adsorbed on the N-modified carbon surface (Figure S11). The dense ionomer layer ejected water from within the layer. Despite the difference in the thickness of the dense ionomer layer, the formation of a dense ionomer layer near the carbon surface is consistent with the findings of the NR experiments. Additionally, the disappearance of water from the dense ionomer layer at the N-modified carbon surface was reproduced in the MD simulations. However, as revealed by MD simulation, the water-rich layer at the topmost surface of the N-modified carbon could not be identified using the NR profiles because of limited resolution and the roughness of the carbon surface. Therefore, we revisited the NR fitting based on the results of the MD calculations. The model with a 5-Å-thick water-rich layer on the topmost carbon surface was reexamined in the fitting of NR data, but we noted that no significantly different results were obtained. It is worth noting that whereas densification of ionomer at Pt−Nafion interface has also been predicted and measured from earlier studies,[18−20] the Pt−Nafion interface is also enriched in interfacial water and could not be identified by NR analysis.[20]

Yang et al.[55] reported that the ζ-potential of carbon black varied from −1.28 to +74.2 mV when N functional groups were introduced to the carbon support for use in catalyst layers. In the simulation reported herein, only the surface charge derived from the quaternary N group (Figure S4b) was assigned to the N-modified carbon surface, which corresponded to a ζ-potential of approximately +25 mV (see the Experimental Section). The positive charge generated by the ionization of the quaternary N group was sufficient to attract the SO_3^- group in the side chains of the Nafion ionomers. A hydrophobic as-deposited carbon surface with a positive charge identical to that of the N-modified carbon surface was also simulated (Figure 8c), and the results were similar to those of the N-modified carbon surface. Therefore, a positively ionized surface was found to play a role in attracting the negatively charged SO_3^- groups via Coulomb interactions.

On the as-deposited carbon surface, the main chain of the Nafion ionomer adsorbs onto the hydrophobic carbon surface via hydrophobic interactions,[51,56,57] leading to the formation of a thin ionomer adsorption layer. In the case of the N-modified carbon surface, the SO_3^- groups in the side chains of the Nafion ionomers are bound to the positively charged surface, which is created by the N functional groups, via Coulombic interactions. Therefore, a thick and dense ionomer adsorption layer is formed at the carbon surface owing to long-range Coulomb interactions.

The interactions between carbon and ionomers, which occupy a large area in the catalyst layer of PEFCs,[58] were targeted in the present study. The effects of the carbon−ionomer interactions on the catalyst layer are discussed henceforth. The rigid ionomer bonding on the N-modified carbon supports presumably suppresses the ionomer poisoning of Pt catalysts in the catalyst layer, resulting in improved PEFC performance upon the use of the N-modified carbon supports in the cathode catalyst layers.[29−36] Furthermore, N-modified carbon supports can reduce the amount of "nonadsorbed ionomers" in catalyst inks,[59] which adversely affects the dispersion stability,[31] viscosity-related properties,[58−60] and the quality of the catalyst layer,[61] emphasizing their potential role in ensuring productivity and durability of PEFCs.

CONCLUSIONS

The vertical ionomer distribution on carbon surfaces modified with nitrogen via NH_3 treatment was investigated by performing NR using the double-contrast method. The NR measurements provided evidence in support of introducing nitrogen to the surface of the carbon supports for preventing ionomer poisoning and the formation of a dense ionomer layer at the Pt−ionomer interface. Specifically, an ∼3-nm-thick Nafion ionomer adsorption layer was observed at the N-modified carbon surface. The density of this compact layer was higher than that of the bulk layer. Moreover, the surface morphologies and chemical composition of the N-modified carbon were investigated by SEM, AFM, XPS, and Raman spectroscopy to validate the NR analysis results. Furthermore, MD simulations revealed that the mechanism of ionomer distribution at the N-modified carbon surface originated from interactions between the positively charged carbon surface and the sulfonic acid groups in the side chains of Nafion ionomers via Coulomb interactions.

EXPERIMENTAL SECTION

Sample Preparation. Approximately 50-nm-thick carbon thin films were deposited on 3-mm-thick Si wafers with a diameter of 2″ by magnetron sputtering. The carbon thin films were fabricated by Kyodo International, Inc., and their surfaces were modified using a previously reported method.[31] To this end, the carbon films were first treated with concentrated HNO_3 (FUJIFILM Wako Pure Chemical) at 70 °C for 2 h and then rinsed three times with ultrapure water to supply carboxylic and hydroxyl groups.[37] We confirmed that the surface on the side of the carbon layer was perfectly wet during the NHO_3 treatment process. The carbon films were subsequently heated in a tube furnace for 2 h with a mixture of NH_3 and Ar gases at flow rates of 0.5 and 0.2 L/min, respectively, to replace O functional groups with N functional groups. We prepared $TiO_{2-x}N_x$ from TiO_2 to check the color distribution upstream and downstream, ensuring that homogeneous chemical reaction occurred upstream and downstream. This fabrication procedure and the sample notations are shown in Figure 1a. Approximately 30-nm-thick ionomer thin films were prepared on the carbon films by spin-coating a Nafion ionomer dispersion at 2000 rpm for 30 s.[40] The D2020 Nafion ionomer dispersion (20 wt %; Chemours) was diluted to 1 wt % using 1-propanol (FUJIFILM Wako Pure Chemical) and used as the dispersion. The films obtained were annealed at 120 °C for 1 h in a vacuum oven.

Characterization of Carbon Thin Films. The surface morphologies of the carbon thin films were examined by field emission SEM (FE-SEM; Regulus SU8230, Hitachi High Technologies) in secondary electron mode at an accelerated voltage of 2 kV. The surface roughness of the carbon thin films was studied using an AFM device (Bruker Dimension ICON) with high-resolution silicon AFM probes (Budget Sensors SHR75, 3 N/m). XPS analysis of the films was performed using monochromatic Al Kα X-rays (1486.6 eV) to determine their chemical compositions. A detector diameter and take-off angle of ∼200 μm and 45°, respectively, were used. All XPS profiles were charge-corrected according to the C 1s main peak of the corresponding samples, which was assigned binding energy of 284.5 eV (Figure S2a). It is worth noting that the carbon films were stored in a vacuum desiccator prior to being analyzed by XPS (Quantera SXM, ULVAC PHI). The XPS analysis was completed within 3 days of sample fabrication. Raman spectra were collected using a laser Raman spectrometer (NRS-3300, Jasco) with 532 nm excitation light.

NR Measurements. NR measurements were performed at BL17 SHARAKU, which is a vertical-type time-of-flight neutron reflectometer at the Japan Proton Accelerator Complex, Material and Life Science Experimental Facility (J-PARC MLF).[62] Neutron pulses of 25 Hz were generated with a wavelength band of 0.2 nm < λ < 0.88 nm.

https://doi.org/10.1021/acsami.2c14574
ACS Appl. Mater. Interfaces 2022, 14, 53744−53754

Reflectometry profiles were obtained at reflection angles of 0.3, 0.7, 1.6, and 3.5°, covering a q-range of 0.07−3.0 nm^{-1}. The magnitude of the scattering vector q was defined as $4\pi\sin\theta/\lambda$, where θ (rad) is the incident angle. All measurements were performed for approximately 1.5 h to obtain sufficient counting statistics. The collected data were analyzed using the Motofit macro package Igor Pro.[63] The NR experiments were performed with two scattering contrasts on the same system using H_2O and D_2O (double-contrast measurements).[20,40,41] This method enabled quantitative evaluation of the water content penetrating the Nafion ionomer thin film. The NR measurements were performed at room temperature (22 °C) and under controlled RH conditions as follows: H_2O vapor, dry N_2 at 4% RH, D_2O vapor, and dry N_2 at 4% RH. Saturated KCl in H_2O/D_2O was added to a homemade aluminum airtight cell that could hold all five samples to maintain wet conditions (85% RH). To achieve dry conditions, N_2 gas was supplied to the cell at a flow rate of 0.1 L/min. The temperature and humidity inside the cells were monitored throughout the measurements. An equilibration time of at least 1 h was used each time the cell was opened before initiating the reflectivity measurements.

MD Simulations. A periodic slab model of a wet Nafion ionomer on a graphite layer with saturated KCl solution buffer was used as the simulation system (Figure S8a). The thicknesses of the graphite layer, ionomer, and buffer were 3, 9, and 6 nm, respectively. A 7-nm-thick gas layer was placed between the ionomer and buffer. The total volume of the simulation cell was 5.112 × 4.919 × 25 nm^3. To investigate the effects of nitrogen modification on ionomer adsorption, pure and quaternary N-functionalized graphite layers were modeled as the as-deposited and N-modified carbon surfaces, respectively. As shown in Figure S8b, 64 carbon atoms were exchanged for quaternary N functional groups in the outermost N-modified graphite layer on the side of the Nafion ionomer. The atomic exchange ratio of nitrogen to carbon was 1/15, which corresponded to the number of quaternary N functional groups in Film N600, as determined by XPS analysis (Figure S4b). Here, the XPS measurements were presumed to help determine the chemical compositions of the top 10 layers of graphite sheets (~3.4 nm). When the N-modified carbon surface encountered the Nafion ionomer film, the quaternary N functional groups were completely ionized with a total charge of +64e. This surface charge was estimated to be approximately +25 mV in terms of ζ-potential (see the Supporting Information). In this system, the Nafion ionomer was modeled as an infinite-chain polymer (equivalent weight = 1044) consisting of 203 monomers. The sulfonic acid in the ionomer is unlikely to be dissociated below λ = 3, as discussed by Kusoglu and Weber,[64] but all sulfonic acid groups in the ionomer were treated as dissociated in our calculation. The ionomer film contains $203 - N^{\text{nitrogen}}$ hydronium ions and round$(203(\lambda_W - 1))$ water molecules, where N^{nitrogen} is the number of quaternary N functional groups in the outermost graphite layer, and round(x) is the rounding-off function. In this setting, the total charge of the system was zero. The KCl buffer, which contains 5000 H_2O molecules, 296 K ions, and 296 Cl ions, helped control the humidity and shielded against the electrostatic effects from adjacent cells. The details of the force fields and basic MD settings are shown in the Supporting Information.

To create the periodic structure for the simulations, graphite, Nafion ionomer, and KCl buffer layers were prepared separately. The graphite layers were created using an in-house program. Overall, nine layers that were 0.335 nm apart were constructed. To create the N-modified graphite layer, the carbon atoms were manually exchanged for nitrogen atoms. The Nafion ionomer layer was created as follows: (i) A three-dimensional monomer structure was constructed using OpenBabel[65] from the SMILES strings[66] of the fluorine-terminated monomer. (ii) The monomer main chain was straightened using a 100 ps MD simulation with a 2000 kJ/(mol nm) repulsive force between the terminals. (iii) The terminals were removed, and the monomer was duplicated periodically to create a straight infinite-chain polymer. The charges on the terminal fluorine atoms were moved to the adjacent carbon atoms. (iv) Hydronium ions and water molecules were added randomly to avoid overlap between atoms and walls, which are described in the next step. (v) The Nafion ionomer system, which was a cell with a volume of 5.112 × 4.919 × 9 nm^3, was deformed using MD simulations with z-directional wall potentials. The Coulomb interactions were turned off in the deformation and turned on during the succeeding 100 ps relaxation in the constant-pressure (1 bar) MD calculations. (vi) The Nafion ionomer system was annealed 30 times according to the literature.[67−69] The following procedure was employed for the annealing: (a) heating from 300 to 1000 K over 100 ps at constant volume; (b) relaxing for 100 ps at 1000 K under constant-volume conditions; (c) cooling from 1000 to 300 K over 100 ps at constant volume; and (d) relaxing for 100 ps at 300 K at constant pressure (1 bar). The volume was confirmed to remain almost constant during the annealing cycle. To create the KCl buffer, water molecules and ions were randomly placed in a periodic cell with a volume of 5.112 × 4.919 × 20 nm^3 and subsequently deformed in the z-direction to 6 nm in a 200 ps MD simulation with the wall potential. An additional 100 ps constant-volume relaxation was performed thereafter. A 1 nm cutoff was used for the Coulombic interactions in this operation.

After the various components were created, they were docked using an in-house program. Then, a 22.2 ns simulation was performed for the relaxation, followed by a 200 ns calculation for the distribution of each component under constant-volume conditions at 300 K. Time steps of 0.02 and 2 fs were used in the initial 200 ps relaxation and the remaining simulations, respectively. The λ_W values were set to 2.4 and 4.0 to obtain the data shown in Figure 8a−8c, respectively. Water distribution was calculated using the MDAnalysis package.[70]

■ ASSOCIATED CONTENT

Supporting Information

The Supporting Information is available free of charge at https://pubs.acs.org/doi/10.1021/acsami.2c14574.

Roughness parameters acquired from AFM images; water contact angle; XPS profiles; NR spectra under dry conditions; detailed fitting procedure and summary of fitting parameters; carbon roughness correction for NR analysis; density changes in carbon layer; estimation of surface charge; and details concerning the MD simulations (PDF)

■ AUTHOR INFORMATION

Corresponding Authors

Wataru Yoshimune − *Toyota Central R&D Labs, Inc., Nagakute, Aichi 480-1192, Japan;* orcid.org/0000-0001-8768-0122; Email: e1707@mosk.tytlabs.co.jp

Nobuaki Kikkawa − *Toyota Central R&D Labs, Inc., Nagakute, Aichi 480-1192, Japan;* orcid.org/0000-0002-8351-4060; Email: kikkawa@mosk.tytlabs.co.jp

Authors

Hiroaki Yoneyama − *Toyota Central R&D Labs, Inc., Nagakute, Aichi 480-1192, Japan*

Naoko Takahashi − *Toyota Central R&D Labs, Inc., Nagakute, Aichi 480-1192, Japan*

Saori Minami − *Toyota Central R&D Labs, Inc., Nagakute, Aichi 480-1192, Japan*

Yusuke Akimoto − *Toyota Central R&D Labs, Inc., Nagakute, Aichi 480-1192, Japan*

Takuya Mitsuoka − *Toyota Central R&D Labs, Inc., Nagakute, Aichi 480-1192, Japan*

Hiroyuki Kawaura − *Toyota Central R&D Labs, Inc., Nagakute, Aichi 480-1192, Japan;* orcid.org/0000-0002-6805-8124

Masashi Harada − *Toyota Central R&D Labs, Inc., Nagakute, Aichi 480-1192, Japan;* orcid.org/0000-0002-0263-6702

Norifumi L. Yamada − *Institute of Materials Structure Science, High Energy Accelerator Research Organization, Naka-gun, Ibaraki 319-1106, Japan;* orcid.org/0000-0002-8370-4526

Hiroyuki Aoki − *Institute of Materials Structure Science, High Energy Accelerator Research Organization, Naka-gun, Ibaraki 319-1106, Japan; Materials and Life Science Division, J-PARC Center, Japan Atomic Energy Agency, Naka-gun, Ibaraki 319-1195, Japan;* orcid.org/0000-0001-7521-2743

Complete contact information is available at: https://pubs.acs.org/10.1021/acsami.2c14574

Author Contributions

W.Y. outlined the research, prepared the samples, conducted the NR measurements, and wrote the manuscript. N.K. and S.M. performed the MD simulations. H.Y. and N.T. performed the Raman and XPS investigations, respectively, and analyzed the corresponding spectra. Y.A. and T.M. captured the SEM and AFM images, respectively. H.K., H.M., N.L.Y., and H.A. conducted investigations to support the NR measurements and discussed the obtained data. All authors, mainly H.A., have reviewed and revised the manuscript. All authors approved the final version of the manuscript.

Notes

The authors declare no competing financial interest.

■ ACKNOWLEDGMENTS

The neutron reflectometry experiments were performed at the Materials and Life Science Experimental Facility of J-PARC under a user program (Proposal No. 2019L0402). The authors are grateful to Dr. Shu Saeki (Toyota Central R&D Labs, Inc.) and Dr. Noboru Miyata [Comprehensive Research Organization for Science and Society (CROSS)] for their support with the NH_3 treatment and NR measurements, respectively.

■ REFERENCES

(1) Kodama, K.; Nagai, T.; Kuwaki, A.; Jinnouchi, R.; Morimoto, Y. Challenges in Applying Highly Active Pt-Based Nanostructured Catalysts for Oxygen Reduction Reactions to Fuel Cell Vehicles. *Nat. Nanotechnol.* **2021**, *16*, 140−147.

(2) Yoshida, T.; Kojima, K. Toyota MIRAI Fuel Cell Vehicle and Progress Toward a Future Hydrogen Society. *Interface Mag.* **2015**, *24*, 45−49.

(3) Pan, L.; Ott, S.; Dionigi, F.; Strasser, P. Current Challenges Related to the Deployment of Shape-Controlled Pt Alloy Oxygen Reduction Reaction Nanocatalysts into Low Pt-Loaded Cathode Layers of Proton Exchange Membrane Fuel Cells. *Curr. Opin. Electrochem.* **2019**, *18*, 61−71.

(4) Fan, J.; Chen, M.; Zhao, Z.; Zhang, Z.; Ye, S.; Xu, S.; Wang, H.; Li, H. Bridging the Gap Between Highly Active Oxygen Reduction Reaction Catalysts and Effective Catalyst Layers for Proton Exchange Membrane Fuel Cells. *Nat. Energy* **2021**, *6*, 475−486.

(5) Sun, Y.; Polani, S.; Luo, F.; Ott, S.; Strasser, P.; Dionigi, F. Advancements in Cathode Catalyst and Cathode Layer Design for Proton Exchange Membrane Fuel Cells. *Nat. Commun.* **2021**, *12*, No. 5984.

(6) He, D.; Cheng, K.; Peng, T.; Sun, X.; Pan, M.; Mu, S. Bifunctional Effect of Reduced Graphene Oxides to Support Active Metal Nanoparticles for Oxygen Reduction Reaction and Stability. *J. Mater. Chem.* **2012**, *22*, 21298−21304.

(7) He, D.; Jiang, Y.; Lv, H.; Pan, M.; Mu, S. Nitrogen-Doped Reduced Graphene Oxide Supports for Noble Metal Catalysts with Greatly Enhanced Activity and Stability. *Appl. Catal., B* **2013**, *132-133*, 379−388.

(8) Zhao, X.; Hamamura, Y.; Yoshida, Y.; Kaneko, T.; Gunji, T.; Takao, S.; Higashi, K.; Uruga, T.; Iwasawa, Y. Plasma-Devised Pt/C Model Electrodes for Understanding the Doubly Beneficial Roles of a Nanoneedle-Carbon Morphology and Strong Pt-Carbon Interface in the Oxygen Reduction Reaction. *ACS Appl. Energy Mater.* **2020**, *3*, 5542−5551.

(9) Zhao, X.; Gunji, T.; Kaneko, T.; Takao, S.; Sakata, T.; Higashi, K.; Yoshida, Y.; Ge, J.; Liu, C.; Xing, W.; Zhu, J.; Xiao, M.; Uruga, T.; Tao, F.; Chen, Z. Evidence for Interfacial Geometric Interactions at Metal−Support Interfaces and their Influence on the Electroactivity and Stability of Pt Nanoparticles. *J. Mater. Chem. A* **2020**, *8*, 1368−1377.

(10) Subbaraman, R.; Strmcnik, D.; Stamenkovic, V.; Markovic, N. M. Three Phase Interfaces at Electrified Metal-Solid Electrolyte Systems 1. Study of the Pt(*hkl*)-Nafion Interface. *J. Phys. Chem. C* **2010**, *114*, 8414−8422.

(11) Jinnouchi, R.; Hatanaka, T.; Morimoto, Y.; Osawa, M. First Principles Study of Sulfuric Acid Anion Adsorption on a Pt (111) Electrode. *Phys. Chem. Chem. Phys.* **2012**, *14*, 3208−3218.

(12) Kodama, K.; Jinnouchi, R.; Suzuki, T.; Murata, H.; Hatanaka, T.; Morimoto, Y. Increase in Adsorptivity of Sulfonate Anions on Pt (111) Surface with Drying of Ionomer. *Electrochem. Commun.* **2013**, *36*, 26−28.

(13) Kodama, K.; Motobayashi, K.; Shinohara, A.; Hasegawa, N.; Kudo, K.; Jinnouchi, R.; Osawa, M.; Morimoto, Y. Effect of the Side-Chain Structure of Perfluoro-Sulfonic Acid Ionomers on the Oxygen Reduction Reaction on the Surface of Pt. *ACS Catal.* **2018**, *8*, 694−700.

(14) Cheng, N.; Mu, S.; Pan, M.; Edwards, P. P. Improved Lifetime of PEM Fuel Cell Catalysts through Polymer Stabilization. *Electrochem. Commun.* **2009**, *11*, 1610−1614.

(15) Cheng, N.; Mu, S.; Chen, X.; Lv, H.; Pan, M.; Edwards, P. P. Enhanced Life of Proton Exchange Membrane Fuel Cell Catalysts using Perfluorosulfonic Acid Stabilized Carbon Support. *Electrochim. Acta* **2011**, *56*, 2154−2159.

(16) He, D.; Mu, S.; Pan, M. Perfluorosulfonic Acid-Functionalized Pt/carbon Nanotube Catalysts with Enhanced Stability and Performance for Use in Proton Exchange Membrane Fuel Cells. *Carbon* **2011**, *49*, 82−88.

(17) He, D.; Kou, Z.; Xiong, Y.; Cheng, K.; Chen, X.; Pan, M.; Mu, S. Simultaneous Sulfonation and Reduction of Graphene Oxide as Highly Efficient Supports for Metal Nanocatalysts. *Carbon* **2014**, *66*, 312−319.

(18) Kudo, K.; Jinnouchi, R.; Morimoto, Y. Humidity and Temperature Dependences of Oxygen Transport Resistance of Nafion Thin Film on Platinum Electrode. *Electrochim. Acta* **2016**, *209*, 682−690.

(19) Jinnouchi, R.; Kudo, K.; Kitano, N.; Morimoto, Y. Molecular Dynamics Simulations on O_2 Permeation through Nafion Ionomer on Platinum Surface. *Electrochim. Acta* **2016**, *188*, 767−776.

(20) Harada, M.; Kudo, K.; Yamada, N. L. Compositional Segregation in a Cross Section of Wet Nafion Thin Film on a Platinum Surface. *Chem. Lett.* **2019**, *48*, 51−54.

(21) Greszler, T. A.; Caulk, D.; Sinha, P. The Impact of Platinum Loading on Oxygen Transport Resistance. *J. Electrochem. Soc.* **2012**, *159*, F831−F840.

(22) Debe, M. K. Electrocatalyst Approaches and Challenges for Automotive Fuel Cells. *Nature* **2012**, *486*, 43−51.

(23) Sinha, P. K.; Gu, W.; Kongkanand, A.; Thompson, E. Performance of Nano Structured Thin Film (NSTF) Electrodes under Partially-Humidified Conditions. *J. Electrochem. Soc.* **2011**, *158*, No. B831.

(24) Yarlagadda, V.; Carpenter, M. K.; Moylan, T. E.; Kukreja, R. S.; Koestner, R.; Gu, W.; Thompson, L.; Kongkanand, A. Boosting Cell Performance with Accessible Carbon Mesopores. *ACS Energy Lett.* **2018**, *3*, 618−621.

(25) Rolfi, A.; Oldani, C.; Merlo, L.; Facchi, D.; Ruffo, R. New Perfluorinated Ionomer with Improved Oxygen Permeability for

Application in Cathode Polymeric Electrolyte Membrane Fuel Cell. *J. Power Sources* **2018**, *396*, 95−101.
(26) Katzenberg, A.; Chowdhury, A.; Fang, M.; Weber, A. Z.; Okamoto, Y.; Kusoglu, A.; Modestino, M. Highly Permeable Perfluorinated Sulfonic Acid Ionomers for Improved Electrochemical Devices: Insights into Structure-Property Relationships. *J. Am. Chem. Soc.* **2020**, *142*, 3742−3752.
(27) Katzenberg, A.; Mukherjee, D.; Dudenas, P. J.; Okamoto, Y.; Kusoglu, A.; Modestino, M. A. Dynamic Emergence of Nanostructure and Transport Properties in Perfluorinated Sulfonic Acid Ionomers. *Macromolecules* **2020**, *53*, 8519−8528.
(28) Jinnouchi, R.; Kudo, K.; Kodama, K.; Kitano, N.; Suzuki, T.; Minami, S.; Shinozaki, K.; Hasegawa, N.; Shinohara, A. The Role of Oxygen-Permeable Ionomer for Polymer Electrolyte Fuel Cells. *Nat. Commun.* **2021**, *12*, No. 4956.
(29) Orfanidi, A.; Madkikar, P.; El-Sayed, H. A.; Harzer, G. S.; Kratky, T.; Gasteiger, H. A. The Key to High Performance Low Pt Loaded Electrodes. *J. Electrochem. Soc.* **2017**, *164*, F418−F426.
(30) Harzer, G. S.; Orfanidi, A.; El-Sayed, H.; Madkikar, P.; Gasteiger, H. A. Tailoring Catalyst Morphology towards High Performance for Low Pt Loaded PEMFC Cathodes. *J. Electrochem. Soc.* **2018**, *165*, F770−F779.
(31) Ott, S.; Orfanidi, A.; Schmies, H.; Anke, B.; Nong, H. N.; Hübner, J.; Gernert, U.; Gliech, M.; Lerch, M.; Strasser, P. Ionomer Distribution Control in Porous Carbon-Supported Catalyst Layers for High-Power and Low Pt-Loaded Proton Exchange Membrane Fuel Cells. *Nat. Mater.* **2020**, *19*, 77−85.
(32) Fang, Z.; Lee, M. S.; Kim, J. Y.; Kim, J. H.; Fuller, T. F. The Effect of Carbon Support Surface Functionalization on PEM Fuel Cell Performance, Durability, and Ionomer Coverage in the Catalyst Layer. *J. Electrochem. Soc.* **2020**, *167*, No. 064506.
(33) Matsutori, K.; Olu, P. Y.; Matsuoka, M.; Nakazawa, T.; Kinumoto, T. Carbon Black Functionalized by Grafting of Azo-Generated-Radicals as Electrocatalyst Support for the Oxygen Reduction Reaction. *Electrochem. Sci. Adv.* **2021**, *1*, No. e2100014.
(34) Ott, S.; Du, F.; Luna, M. L.; Dao, T. A.; Selve, S.; Cuenya, B. R.; Orfanidi, A.; Strasser, P. Property-Reactivity Relations of N-doped PEM Fuel Cell Cathode Catalyst Supports. *Appl. Catal., B* **2022**, *306*, No. 121118.
(35) Hornberger, E.; Merzdorf, T.; Schmies, H.; Hübner, J.; Klingenhof, M.; Gernert, U.; Kroschel, M.; Anke, B.; Lerch, M.; Schmidt, J.; Thomas, A.; Chattot, R.; Martens, I.; Drnec, J.; Strasser, P. Impact of Carbon N-Doping and Pyridinic-N Content on the Fuel Cell Performance and Durability of Carbon-Supported Pt Nanoparticle Catalysts. *ACS Appl. Mater. Interfaces* **2022**, *14*, 18420−18430.
(36) Islam, M. N.; Basha, A. B. M.; Kollath, V. O.; Soleymani, A. P.; Jankovic, J.; Karan, K. Designing Fuel Cell Catalyst Support for Superior Catalytic Activity and Low Mass-Transport Resistance. *Nat. Commun.* **2022**, *13*, No. 6157.
(37) Kundu, S.; Wang, Y.; Xia, W.; Muhler, M. Thermal Stability and Reducibility of Oxygen-Containing Functional Groups on Multiwalled Carbon Nanotube Surfaces: A Quantitative High-Resolution XPS and TPD/TPR Study. *J. Phys. Chem. C* **2008**, *112*, 16869−16878.
(38) Du, F.; Dao, T. A.; Peitl, P. V. J.; Bauer, A.; Preuss, K.; Bonastre, A. M.; Sharman, J.; Spikes, G.; Perchthaler, M.; Schmidt, T. J.; Orfanidi, A. Effects of PEMFC Operational History under Dry/Wet Conditions on Additional Voltage Losses due to Ionomer Migration. *J. Electrochem. Soc.* **2020**, *167*, No. 144513.
(39) Paul, D. K.; Karan, K. Conductivity and Wettability Changes of Ultrathin Nafion Films Subjected to Thermal Annealing and Liquid Water Exposure. *J. Phys. Chem. C* **2014**, *118*, 1828−1835.
(40) Ito, K.; Harada, M.; Yamada, N. L.; Kudo, K.; Aoki, H.; Kanaya, T. Water Distribution in Nafion Thin Films on Hydrophilic and Hydrophobic Carbon Substrates. *Langmuir* **2020**, *36*, 12830−12837.
(41) DeCaluwe, S. C.; Kienzle, P. A.; Bhargava, P.; Baker, A. M.; Dura, J. A. Phase Segregation of Sulfonate Groups in Nafion Interface Lamellae, Quantified via Neutron Reflectometry Fitting Techniques for Multi-Layered Structures. *Soft Matter* **2014**, *10*, 5763−5776.
(42) Dura, J. A.; Murthi, V. S.; Hartman, M.; Satija, S. K.; Majkrzak, C. F. Multilamellar Interface Structures in Nafion. *Macromolecules* **2009**, *42*, 4769−4774.
(43) Eastman, S. A.; Kim, S.; Page, K. A.; Rowe, B. W.; Kang, S.; DeCaluwe, S. C.; Dura, J. A.; Soles, C. L.; Yager, K. G. Effect of Confinement on Structure, Water Solubility, and Water Transport in Nafion Thin Films. *Macromolecules* **2012**, *45*, 7920−7930.
(44) Kawamoto, T.; Aoki, M.; Kimura, T.; Chinapang, P.; Mizusawa, T.; Yamada, N. L.; Nemoto, F.; Watanabe, T.; Tanida, H.; Matsumoto, M.; Imai, H.; Miyake, J.; Miyatake, K.; Inukai, J. Sublayered Structures of Hydrated Nafion Thin Film Formed by Casting on Pt Substrate Analyzed by X-Ray Absorption Spectroscopy under Ambient Conditions and Neutron Reflectometry at Temperature of 80 °C and Relative Humidity of 30−80%. *Electrochemistry* **2019**, *87*, 270−275.
(45) Kawamoto, T.; Aoki, M.; Kimura, T.; Mizusawa, T.; Yamada, N. L.; Miyake, J.; Miyatake, K.; Inukai, J. In-Plane Distribution of Water inside Nafion Thin Film Analyzed by Neutron Reflectivity at Temperature of 80 °C and Relative Humidity of 30%−80% Based on 4-Layered Structural Model. *Jpn. J. Appl. Phys.* **2019**, *58*, No. SIID01.
(46) Kim, S.; Dura, J. A.; Page, K. A.; Rowe, B. W.; Yager, K. G.; Lee, H.-J.; Soles, C. L. Surface-Induced Nanostructure and Water Transport of Thin Proton-Conducting Polymer Films. *Macromolecules* **2013**, *46*, 5630−5637.
(47) Shrivastava, U. N.; Fritzsche, H.; Karan, K. Interfacial and Bulk Water in Ultrathin Films of Nafion, 3M PFSA, and 3M PFIA Ionomers on a Polycrystalline Platinum Surface. *Macromolecules* **2018**, *51*, 9839−9849.
(48) Shrivastava, U. N.; Suetsugu, K.; Nagano, S.; Fritzsche, H.; Nagao, Y.; Karan, K. Cross-Correlated Humidity-Dependent Structural Evolution of Nafion Thin Films Confined on a Platinum Substrate. *Soft Matter* **2020**, *16*, 1190−1200.
(49) Wang, X.; Shi, G. An Introduction to the Chemistry of Graphene. *Phys. Chem. Chem. Phys.* **2015**, *17*, 28484−28504.
(50) Iwase, H.; Sawada, S.-i.; Yamaki, T.; Maekawa, Y.; Koizumi, S. Preirradiation Graft Polymerization of Styrene in a Poly(tetrafluoroethylene) Film Investigated by Time-Resolved Small-Angle Neutron Scattering. *Int. J. Polym. Sci.* **2011**, *2011*, No. 301807.
(51) Mashio, T.; Malek, K.; Eikerling, M.; Ohma, A.; Kanesaka, H.; Shinohara, K. Molecular Dynamics Study of Ionomer and Water Adsorption at Carbon Support Materials. *J. Phys. Chem. C* **2010**, *114*, 13739−13745.
(52) Kusoglu, A.; Savagatrup, S.; Clark, K. T.; Weber, A. Z. Role of Mechanical Factors in Controlling the Structure−Function Relationship of PFSA Ionomers. *Macromolecules* **2012**, *45*, 7467−7476.
(53) Karan, K. Interesting Facets of Surface, Interfacial, and Bulk Characteristics of Perfluorinated Ionomer Films. *Langmuir* **2019**, *35*, 13489−13520.
(54) Mabuchi, T.; Huang, S. F.; Tokumasu, T. Influence of Ionomer Loading and Substrate Wettability on the Morphology of Ionomer Thin Films Using Coarse-Grained Solvent Evaporation Simulations. *Macromolecules* **2021**, *54*, 115−125.
(55) Yang, F.; Xin, L.; Uzunoglu, A.; Qiu, Y.; Stanciu, L.; Ilavsky, J.; Li, W.; Xie, J. Investigation of the Interaction between Nafion Ionomer and Surface Functionalized Carbon Black Using Both Ultrasmall Angle X-ray Scattering and Cryo-TEM. *ACS Appl. Mater. Interfaces* **2017**, *9*, 6530−6538.
(56) Yoshimune, W.; Harada, M. Effect of Pt Loading on the Adsorption of Perfluoro-sulfonic Acid Ionomer in Catalyst Ink for Polymer Electrolyte Fuel Cells. *Chem. Lett.* **2019**, *48*, 487−490.
(57) Guo, Y.; Mabuchi, T.; Li, G.; Tokumasu, T. Morphology Evolution and Adsorption Behavior of Ionomers from Solution to Pt/C Substrates. *Macromolecules* **2022**, *55*, 4245−4255.
(58) Balu, R.; Choudhury, N. R.; Mata, J. P.; de Campo, L.; Rehm, C.; Hill, A. J.; Dutta, N. K. Evolution of the Interfacial Structure of a Catalyst Ink with the Quality of the Dispersing Solvent: A Contrast

Variation Small-Angle and Ultrasmall-Angle Neutron Scattering Investigation. *ACS Appl. Mater. Interfaces* **2019**, *11*, 9934−9946.
(59) Yoshimune, W.; Harada, M. Impact of Nonadsorbed Ionomer on Viscosity of Catalyst Inks for Polymer Electrolyte Fuel Cells. *Bull. Chem. Soc. Jpn.* **2020**, *93*, 302−307.
(60) Yoshimune, W.; Harada, M. Temperature-Induced Shear-thinning in Catalyst Inks. *Electrochem. Commun.* **2021**, *130*, No. 107099.
(61) Harada, M.; Takata, S.-i.; Iwase, H.; Kajiya, S.; Kadoura, H.; Kanaya, T. Distinguishing Adsorbed and Deposited Ionomers in the Catalyst Layer of Polymer Electrolyte Fuel Cells Using Contrast-Variation Small-Angle Neutron Scattering. *ACS Omega* **2021**, *6*, 15257−15263.
(62) Takeda, M.; Yamazaki, D.; Soyama, K. Current Status of a New Polarized Neutron Reflectometer at the Intense Pulsed Neutron Source of the Materials and Life Science Experimental Facility (MLF) of J-PARC. *Chin. J. Phys.* **2012**, *50*, 161−170.
(63) Nelson, A. Co-Refinement of Multiple-Contrast Neutron/X-ray Reflectivity Data Using MOTFIT. *J. Appl. Crystallogr.* **2006**, *39*, 273−276.
(64) Kusoglu, A.; Weber, A. Z. New Insights into Perfluorinated Sulfonic-Acid Ionomers. *Chem. Rev.* **2017**, *117*, 987−1104.
(65) O'Boyle, N. M.; Banck, M.; James, C. A.; Morley, C.; Vandermeersch, T.; Hutchison, G. R. Open Babel: An Open Chemical Toolbox. *J. Cheminf.* **2011**, *3*, No. 33.
(66) Weininger, D. SMILES, a Chemical Language and Information System. 1. Introduction to Methodology and Encoding Rules. *J. Chem. Inf. Model.* **1988**, *28*, 31−36.
(67) Mashio, T.; Ohma, A.; Tokumasu, T. Molecular Dynamics Study of Ionomer Adsorption at a Carbon Surface in Catalyst Ink. *Electrochim. Acta* **2016**, *202*, 14−23.
(68) Nakauchi, M.; Mabuchi, T.; Yoshimoto, Y.; Hori, T.; Kinefuchi, I.; Takeuchi, H.; Tokumasu, T. Molecular Dynamics Study of Oxygen Scattering Behavior on Perfluorosulfonic Acid Ionomer Thin Films. *J. Phys. Chem. C* **2019**, *123*, 7125−7133.
(69) Zhang, X.-y.; Ding, Y.-h. Thickness-Dependent Structural and Transport Behaviors in the Platinum-Nafion Interface: A Molecular Dynamics Investigation. *RSC Adv.* **2014**, *4*, 44214−44222.
(70) Michaud-Agrawal, N.; Denning, E. J.; Woolf, T. B.; Beckstein, O. MDAnalysis: A Toolkit for the Analysis of Molecular Dynamics Simulations. *J. Comput. Chem.* **2011**, *32*, 2319−2327.

https://doi.org/10.1021/acsami.2c14574
ACS Appl. Mater. Interfaces 2022, 14, 53744−53754